

Netherlands  
organization for  
applied scientific  
research

TNO-report



TNO Physics and Electronics  
Laboratory

P.O. Box 96864  
2509 JG The Hague  
Oude Waalsdorperweg 63  
The Hague, The Netherlands  
Fax +31 70 328 09 61  
Phone +31 70 326 42 21



report no.  
FEL-92-B190

copy no.

8

title

Theory and applications of the 3-dimensional  
finite-difference time-domain method

**AD-A256 559**



Nothing from this issue may be reproduced  
and/or published by print, photoprint,  
microfilm or any other means without  
previous written consent from TNO.  
Submitting the report for inspection to  
parties directly interested is permitted.

In case this report was drafted under  
instruction, the rights and obligations  
of contracting parties are subject to either  
the 'Standard Conditions for Research  
Instructions given to TNO' or the relevant  
agreement concluded between the contracting  
parties on account of the research object  
involved.

© TNO

author(s):

G.J.A. van Gennip

date :

June 1992

**DTIC**  
**ELECTE**  
**OCT 29 1992**  
**S A D**

This document has been approved  
for public release and sale; its  
distribution is unlimited.

classification

title

: unclassified

abstract

: unclassified

report text

: unclassified

no. of copies

: 27

no. of pages

: 35 (excl. RDP & distribution list)

appendices

: -

All information which is classified according to  
Dutch regulations shall be treated by the recipient in  
the same way as classified information of  
corresponding value in his own country. No part of  
this information will be disclosed to any party.

**92-28442**



report no. : FEL-92 B190  
title : Theory and applications of the 3-dimensional finite-difference time-domain method  
author(s) : G.J.A. van Gennip  
Institute : TNO Physics and Electronics Laboratory  
date : June 1992  
NDRO no. : -  
no. in pow '92 : 710.5  
Research supervised by: H.J.M. Heemskerk  
Research carried out by: G.J.A. van Gennip

## ABSTRACT (UNCLASSIFIED)

The 3-dimensional finite-difference time-domain method is a numerical method for solving electromagnetic penetration and scattering problems. It uses a finite difference representation of the time dependent Maxwell equations. The object of interest is embedded in a lattice and the time is divided in discrete intervals. By applying the finite-difference equations for every time step the propagation and scattering of waves is simulated. In this report the 3-dimensional FD-TD method and its algorithms are explained. Results are presented for a perfectly conducting plate, cube and wedge and for a dielectric layered sphere. The calculated results agree with experimental and exact theoretical results.



Accession For	
NTIS	CRA&I
DTIC	TAB
Unannounced	
Justification	
By	
Distribution /	
Availability Code	
Dist	Availability Code
A-1	

rapport no. : FEL-92-B190  
titel : Theorie en toepassingen van de 3-dimensionale eindige differentie, tijddomeinmethode  
  
auteur(s) : ir. G.J.A. van Gennip  
instituut : Fysisch en Elektronisch Laboratorium TNO  
  
datum : juni 1992  
hdo-opdr.no. : -  
no. in hwp '92 : 710.5  
  
Onderzoek uitgevoerd o.l.v. : ir. H.J.M. Heemskerk  
Onderzoek uitgevoerd door : ir. G.J.A. van Gennip

---

#### SAMENVATTING (ONGERUBRICEERD)

De 3-dimensionale eindige differentie, tijddomein (finite difference time domain, FD-TD) methode is een numerieke methode om elektromagnetische penetratie- en verstrooiingsproblemen op te lossen. De methode maakt gebruik van een eindige differentie representatie van de tijdafhankelijke vergelijkingen van Maxwell. Het te modelleren object wordt opgenomen in een rooster en de tijd wordt opgedeeld in discrete intervallen. Door toepassing van de eindige differentie vergelijkingen op deze discrete ruimte te herhalen voor elke volgende tijdstap simuleren we de voortplanting en verstrooiing van golven. In dit rapport worden de 3-dimensionale eindige differentie tijd domein methode en de hiervoor benodigde algorithmen behandeld. Resultaten worden gepresenteerd voor een perfect geleidende plaat, kubus en wig en een dielektrisch gelaagde bol. De berekende resultaten komen goed overeen met experimentele en exacte theoretische resultaten.

<b>ABSTRACT</b>	<b>2</b>
<b>SAMENVATTING</b>	<b>3</b>
<b>CONTENTS</b>	<b>4</b>
<b>1 INTRODUCTION</b>	<b>5</b>
<b>2 THEORY AND BASIC ALGORITHMS</b>	<b>6</b>
2.1 Ideas behind the FD-TD method	6
2.2 The algorithms	7
2.2.1 The Yee algorithm	7
2.2.2 Lattice regions and plane wave source condition	10
2.2.3 The lattice truncation condition	12
2.2.4 Sinusoidal steady state	14
2.2.5 The near-to-far field transformation	15
<b>3 FD-TD COMPUTED SCATTERING AND PENETRATION PROBLEMS</b>	<b>17</b>
3.1 Radar cross section of a square metal plate	18
3.2 Radar cross section of a rectangular metal cavity.	20
3.2.1 Vertical polarisation of the incident wave	20
3.2.2 Horizontal polarisation of the incident wave	23
3.3 Radar cross section of a metal wedge	25
3.3.1 Vertical polarisation of incident wave	25
3.3.2 Horizontal polarisation of the incident wave	28
3.4 Field penetration in a lossy inhomogeneous sphere	30
<b>4 CONCLUSIONS</b>	<b>33</b>
<b>LITERATURE</b>	<b>34</b>

## 1 INTRODUCTION

Electromagnetic penetration and scattering problems are usually very complicated. Only a few of them can be solved analytically. For the remainder, one has to use numerical methods. Various methods are being studied at the moment. One of the various methods under consideration is the Finite-Difference, Time-Domain (FD-TD) method.

The FD-TD method uses a finite difference representation of the time dependent Maxwell equations. The object of interest is embedded in a lattice, and time is divided in discrete intervals. By applying the finite difference equations for every time step, we simulate the propagation and scattering of waves. By enforcing a plane wave at  $t = 0$ , subsequent time-stepping will result in a steady state which can be monitored and used to calculate the object's radar cross section.

The main advantage of the FD-TD method is its simplicity. The method can easily be implemented for arbitrary complex objects, because it is possible to designate every cell in the lattice its own material constants.

Chapter two deals with the theory and the used algorithms for the 3-dimensional FD-TD method. It explains the complete method including boundary and source conditions. In chapter three some results are presented and compared with other methods and measurements. The used objects are perfectly conducting plates, cubes and wedges and a dielectric layered sphere.

## 2 THEORY AND BASIC ALGORITHMS

### 2.1 Ideas behind the FD-TD method

The aim of the FD-TD method is to model the propagation of an electromagnetic wave into a volume of space containing a dielectric or conducting object. By time-stepping, i.e. repeatedly implementing a finite difference analog of Maxwell's time-dependent curl equations at each cell of the grid, the incident wave is tracked as it first propagates to the object and then interacts with it. The time-stepping goes on until the sinusoidal steady-state is achieved at all points in the grid.

Time-stepping is done by a finite-difference procedure due to Yee [1]. This procedure requires the positioning of the components of  $\vec{E}$  and  $\vec{H}$  about a unit cell of the lattice as shown in figure 1, and the evaluation of  $\vec{E}$  and  $\vec{H}$  at alternate half-time steps. In this manner a second order accuracy in the space and time increments is attained by using centred finite-difference expressions for both the time and space derivatives.

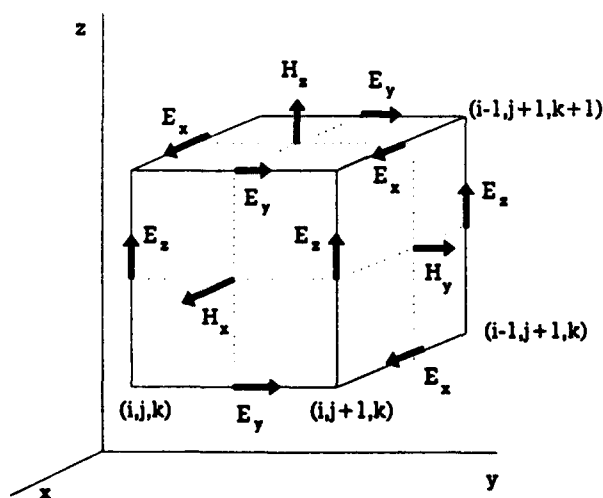


Fig. 1: Positioning of the field components in a space cell

Beside the Yee procedure there are a number of other procedures that need to be developed. The first one is the lattice truncation condition. At the edges of the lattice the centred finite-difference expressions can't be used so that alternative expressions for the edges have to be developed. These expressions are called lattice truncation conditions or absorbing boundary conditions. These conditions must assure that the outgoing waves pass the lattice truncation planes with a minimum of reflections. To minimize computer storage the conditions need to be positioned as close to the object as possible.

The second procedure that is needed is the one that assures that there is a plane wave travelling through the grid. This procedure is called the source condition. This source must not be the cause of any extra reflections as will be the case when the plane wave is simply imposed on a certain plane in the grid.

A third procedure is needed to calculate the radar cross section. Once the fields in the grid have reached the steady state, the near fields are available. These fields will have to be used to calculate the radar cross section. This includes a near-to-far field transformation. In the following paragraphs a detailed discussion is given of the various algorithms.

## 2.2 The algorithms

### 2.2.1 The Yee algorithm

Assuming that  $\epsilon$ ,  $\sigma$ ,  $\mu$  and  $\rho'$  are isotropic, Maxwell's equations in Cartesian coordinates can be denoted as follows

$$\frac{\partial H_x}{\partial t} = \frac{1}{\mu} \left( \frac{\partial E_y}{\partial z} - \frac{\partial E_z}{\partial y} - \rho' H_x \right) \quad (1a)$$

$$\frac{\partial H_y}{\partial t} = \frac{1}{\mu} \left( \frac{\partial E_z}{\partial x} - \frac{\partial E_x}{\partial z} - \rho' H_y \right) \quad (1b)$$

$$\frac{\partial H_z}{\partial t} = \frac{1}{\mu} \left( \frac{\partial E_x}{\partial y} - \frac{\partial E_y}{\partial x} - \rho' H_z \right) \quad (1c)$$

$$\frac{\partial E_x}{\partial t} = \frac{1}{\epsilon} \left( \frac{\partial H_z}{\partial y} - \frac{\partial H_y}{\partial z} - \sigma E_x \right) \quad (1d)$$

$$\frac{\partial E_y}{\partial t} = \frac{1}{\epsilon} \left( \frac{\partial H_x}{\partial z} - \frac{\partial H_z}{\partial x} - \sigma E_y \right) \quad (1e)$$

$$\frac{\partial E_z}{\partial t} = \frac{1}{\epsilon} \left( \frac{\partial H_y}{\partial x} - \frac{\partial H_x}{\partial y} - \sigma E_z \right) \quad (1f)$$

Where  $\epsilon$  is the electrical permittivity in farads/meter;  $\sigma$  is the electrical conductivity in mhos/meter;  $\mu$  is the magnetic permeability in henrys/meter; and  $\rho'$  is an equivalent magnetic resistivity in ohms/meter. The magnetic resistivity term is provided to yield symmetric curl equations, and to allow for the possibility of a magnetic field loss mechanism. In accordance with Yee a point  $(x,y,z) = (i\delta, j\delta, k\delta)$  in space is denoted as  $(i,j,k)$  in which  $\delta = \delta x = \delta y = \delta z$  is the space increment of a cubic lattice. A function  $F(i\delta, j\delta, k\delta, n\Delta t)$  of space and time is denoted as  $F^n(i,j,k)$  in which  $\Delta t$  is the time increment and  $i, j, k$ , and  $n$  are integers. Yee used centred finite-difference expressions for space and time derivatives that are second order accurate in  $\delta$  and  $\Delta t$  respectively.

$$\frac{\partial F^n(i,j,k)}{\partial x} = \frac{F^n(i + \frac{1}{2}, j, k) - F^n(i - \frac{1}{2}, j, k)}{\delta} + O(\delta^2) \quad (2a)$$

$$\frac{\partial F^n(i,j,k)}{\partial t} = \frac{F^{n+\frac{1}{2}}(i,j,k) - F^{n-\frac{1}{2}}(i,j,k)}{\Delta t} + O(\Delta t^2) \quad (2b)$$

Using these expressions to get a finite-difference analog of the Maxwell equations results in

$$\begin{aligned} E_x^{n+1}(i + \frac{1}{2}, j, k) &= C_3(m) E_x^n(i + \frac{1}{2}, j, k) \\ &+ C_4(m) \left( H_z^{n+\frac{1}{2}}(i + \frac{1}{2}, j + \frac{1}{2}, k) - H_z^{n+\frac{1}{2}}(i + \frac{1}{2}, j - \frac{1}{2}, k) \right. \\ &\quad \left. - H_y^{n+\frac{1}{2}}(i + \frac{1}{2}, j, k + \frac{1}{2}) + H_y^{n+\frac{1}{2}}(i + \frac{1}{2}, j, k - \frac{1}{2}) \right) \end{aligned} \quad (3a)$$

$$\begin{aligned} E_y^{n+1}(i, j + \frac{1}{2}, k) &= C_3(m) E_y^n(i, j + \frac{1}{2}, k) \\ &+ C_4(m) \left( H_x^{n+\frac{1}{2}}(i, j + \frac{1}{2}, k + \frac{1}{2}) - H_x^{n+\frac{1}{2}}(i, j + \frac{1}{2}, k - \frac{1}{2}) \right. \\ &\quad \left. - H_z^{n+\frac{1}{2}}(i + \frac{1}{2}, j + \frac{1}{2}, k) + H_z^{n+\frac{1}{2}}(i - \frac{1}{2}, j + \frac{1}{2}, k) \right) \end{aligned} \quad (3b)$$

$$E_z^{n+1}(i, j, k + \frac{1}{2}) = C_3(m)E_z^n(i, j, k + \frac{1}{2}) \quad (3c)$$

$$+ C_4(m) \left( H_y^{n+\frac{1}{2}}(i + \frac{1}{2}, j, k + \frac{1}{2}) - H_y^{n+\frac{1}{2}}(i - \frac{1}{2}, j, k + \frac{1}{2}) \right. \\ \left. - H_x^{n+\frac{1}{2}}(i, j + \frac{1}{2}, k + \frac{1}{2}) + H_x^{n+\frac{1}{2}}(i, j - \frac{1}{2}, k + \frac{1}{2}) \right)$$

$$H_x^{n+\frac{1}{2}}(i, j + \frac{1}{2}, k + \frac{1}{2}) = C_1(m)H_x^{n-\frac{1}{2}}(i, j + \frac{1}{2}, k + \frac{1}{2}) \quad (3d)$$

$$+ C_2(m) \left( E_y^n(i, j + \frac{1}{2}, k + 1) - E_y^n(i, j + \frac{1}{2}, k) \right. \\ \left. - E_z^n(i, j + 1, k + \frac{1}{2}) + E_z^n(i, j, k + \frac{1}{2}) \right)$$

$$H_y^{n+\frac{1}{2}}(i + \frac{1}{2}, j, k + \frac{1}{2}) = C_1(m)H_y^{n-\frac{1}{2}}(i + \frac{1}{2}, j, k + \frac{1}{2}) \quad (3e)$$

$$+ C_2(m) \left( E_z^n(i + 1, j, k + \frac{1}{2}) - E_z^n(i, j, k + \frac{1}{2}) \right. \\ \left. - E_x^n(i + \frac{1}{2}, j, k + 1) + E_x^n(i + \frac{1}{2}, j, k) \right)$$

$$H_z^{n+\frac{1}{2}}(i + \frac{1}{2}, j + \frac{1}{2}, k) = C_1(m)H_z^{n-\frac{1}{2}}(i + \frac{1}{2}, j + \frac{1}{2}, k) \quad (3f)$$

$$+ C_2(m) \left( E_x^n(i + \frac{1}{2}, j + 1, k) - E_x^n(i + \frac{1}{2}, j, k) \right. \\ \left. - E_y^n(i + 1, j + \frac{1}{2}, k) + E_y^n(i, j + \frac{1}{2}, k) \right)$$

with

$$C_1(m) = \frac{2\mu(m) - \Delta t p'(m)}{2\mu(m) + \Delta t p'(m)} \quad (4a)$$

$$C_2(m) = \frac{2\Delta t}{\delta(2\mu(m) + \Delta t p'(m))} \quad (4b)$$

$$C_3(m) = \frac{2\varepsilon(m) - \Delta t \sigma(m)}{2\varepsilon(m) + \Delta t \sigma(m)} \quad (4c)$$

$$C_4(m) = \frac{2\Delta t}{\delta(2\varepsilon(m) + \Delta t \sigma(m))} \quad (4d)$$

in which  $m = \text{media}(i, j, k)$  is the type of medium at a field component location. To ensure stability of this time stepping algorithm,  $\Delta t$  is chosen to satisfy the inequality [2]

$$\Delta t \leq \frac{\delta}{\sqrt{3}c_{\max}} \quad (5)$$

where  $c_{\max}$  is the maximum wave phase velocity within this model.  $\delta$  is chosen to be small compared to the wavelength, usually  $\delta \leq \lambda/10$ . Also  $\delta$  has to be small compared to the dimensions of the object, because curved boundaries are formed by a staircase approximation.

With the system of equations (3a)-(3f), the new value of a field vector component at any lattice point depends only on its previous value and on the previous values of the components of the other field vector at adjacent points. Therefore, at any given time step, the computation of a field vector may proceed either one point at a time, or, with a parallel processing computer, at many points at a time.

### 2.2.2 Lattice regions and plane wave source condition

As shown in figure 2 the FD-TD lattice is divided into two distinct regions, separated by a rectangular surface which serves to connect fields in each region.

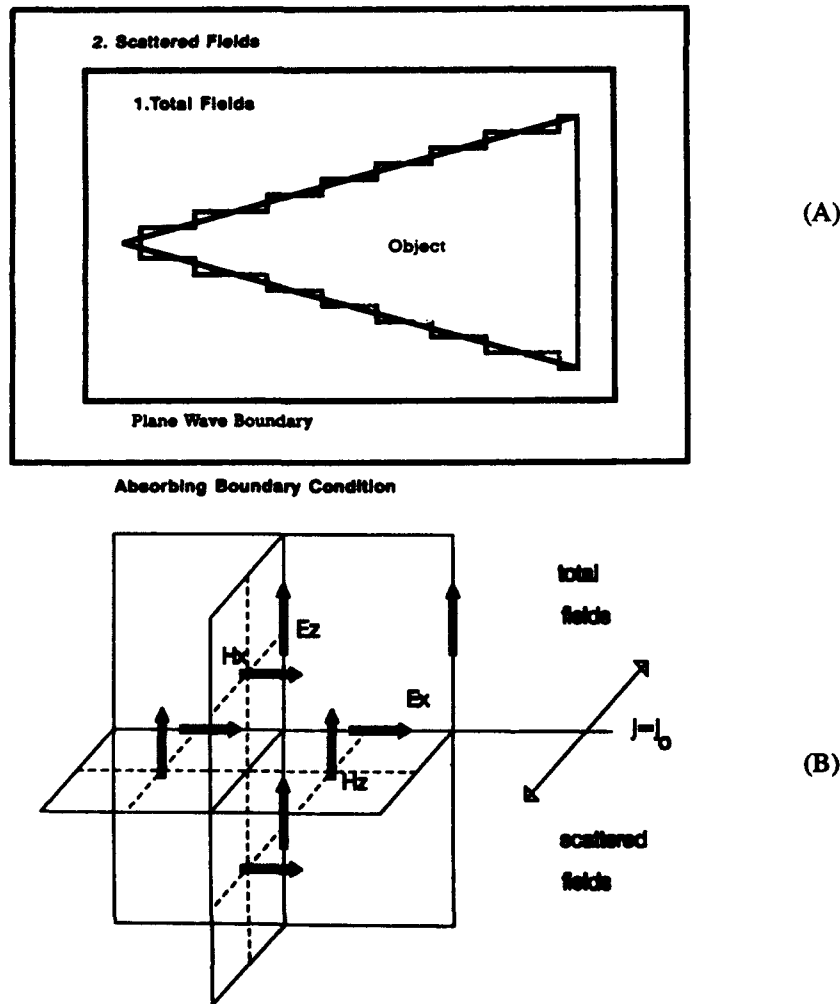


Fig. 2: Division of the lattice into total-field and scattered-field regions (a) global geometry, (b) local geometry

Region 1 of the lattice is denoted the total-field region, region 2 the scattered-field region. The object is positioned in region 1 where all field quantities are comprised of the sum of the incident wave and the scattered field. In region 2 all field quantities are comprised only of the scattered field.

The rectangular planes that form the boundary between regions 1 and 2 contain  $\bar{E}$  and  $\bar{H}$  field components. These field components are updated according to equations (3) and subsequently corrected to maintain the two distinct regions. Typical FD-TD computations at these boundary points are as follows.

$$E_z^{n+1}(i, j_0, k + \frac{1}{2}) = E_z^{n+1}(i, j_0, k + \frac{1}{2})|_{\text{eqn}(3c)} + C_4(m)H_x^{i^{n+\frac{1}{2}}}(i, j_0 - \frac{1}{2}, k + \frac{1}{2}) \quad (6a)$$

$$E_x^{n+1}(i + \frac{1}{2}, j_0, k) = E_x^{n+1}(i + \frac{1}{2}, j_0, k)|_{\text{eqn}(3a)} + C_4(m)H_z^{i^{n+\frac{1}{2}}}(i + \frac{1}{2}, j_0 - \frac{1}{2}, k) \quad (6b)$$

$$H_x^{n+\frac{1}{2}}(i, j_0 - \frac{1}{2}, k + \frac{1}{2}) = H_x^{n+\frac{1}{2}}(i, j_0 - \frac{1}{2}, k + \frac{1}{2})|_{\text{eqn}(3e)} - C_2(m)E_z^{i^n}(i, j_0, k + \frac{1}{2}) \quad (6c)$$

$$H_z^{n+\frac{1}{2}}(i + \frac{1}{2}, j_0 - \frac{1}{2}, k) = H_z^{n+\frac{1}{2}}(i + \frac{1}{2}, j_0 - \frac{1}{2}, k)|_{\text{eqn}(3f)} - C_2(m)E_x^{i^n}(i + \frac{1}{2}, j_0, k) \quad (6d)$$

Here  $E_z^{n+1}(i, j_0, k + \frac{1}{2})$  is the usual FD-TD value of the total  $E_z$  component evaluated at point  $(i, j_0, k + \frac{1}{2})$  and time step  $n+1$ . The superscript "i" denotes the known incident field component value. These computations assure consistency of the subtraction operations of field components across the Region 1 / Region 2 boundary. In effect, total-field quantities are always subtracted from similar total-field quantities; the same goes for scattered-field quantities. This enforcement of consistency serves to precisely connect the two regions. Further, the inclusion of arbitrary values of  $\bar{E}^i$  and  $\bar{H}^i$  in the consistency relations permits the specification of any desired plane wave of arbitrary angle of incidence and arbitrary polarisation.

There are a number of advantages to this method. For the complete object, the high dynamic range total-field formalism is retained. This permits accurate computations of low-level fields in cavities or shadow regions of the scatterer. A very accurate simulation of the radiation condition is possible due to the scattered-field formalism in the lattice truncation region. An other advantage is that the incident wave contribution need to be computed only for the field components at the rectangular surface connecting Regions 1 and 2. And last, the scattered near field in Region 2 can be easily integrated to derive the far-field scattering and radar cross section, as discussed later.

### 2.2.3 The lattice truncation condition

Most of the electromagnetic field problems are "open" problems, which means that the fields are not restricted to a certain area. To solve these problems with the FD-TD method the field computation zone must be limited, otherwise an unlimited amount of data will have to be stored. The computation zone must be large enough to enclose the object of interest, and a suitable boundary condition on the outer perimeter of the computation zone must be used to simulate the extension of the computation zone to infinity. These conditions are called lattice truncation conditions or absorbing boundary conditions. Care must be taken because these conditions must not cause spurious reflections of outgoing scattered waves and must not cause numerical instability.

The wave equation in free space is

$$\frac{\partial^2 U}{\partial x^2} + \frac{\partial^2 U}{\partial y^2} + \frac{\partial^2 U}{\partial z^2} - \frac{1}{c^2} \frac{\partial^2 U}{\partial t^2} = 0 \quad (7)$$

with  $U = E_x, E_y, E_z, H_x, H_y, H_z$ . In other words

$$L \cdot U = 0 \quad (8)$$

with

$$L = D_x^2 + D_y^2 + D_z^2 - \frac{1}{c^2} D_t^2 \quad (9)$$

and

$$D_\alpha = \frac{\partial}{\partial \alpha} \quad (10)$$

$L$  can be written as  $L^+ \cdot L^-$  with

$$L^\pm = D_x \pm \frac{D_t}{c} \sqrt{1 - S^2} \quad (11)$$

and

$$S = \sqrt{\left(\frac{D_y}{D_{y/c}}\right)^2 + \left(\frac{D_z}{D_{z/c}}\right)^2} \quad (12)$$

It can be proven [3] that

$$L^- \cdot U = 0 \quad (13)$$

applied on all field components at  $x = 0$  assures that all outgoing waves are absorbed. At  $x = h$  a similar expression can be found:

$$L^+ \cdot U = 0 \quad (14)$$

For the numerical implementation of these conditions a Taylor approximation of the square root in the  $L$  operator has to be made.

$$\sqrt{1 - S^2} \approx 1 - \frac{1}{2} S^2 \quad (15)$$

This results in six conditions, one for each face of the boundary surface.

$$\frac{\partial^2 U}{\partial x \partial t} - \frac{1}{c} \frac{\partial^2 U}{\partial t^2} + \frac{c}{2} \frac{\partial^2 U}{\partial y^2} + \frac{c}{2} \frac{\partial^2 U}{\partial z^2} = 0 \quad (x = 0) \quad (16a)$$

$$\frac{\partial^2 U}{\partial x \partial t} + \frac{1}{c} \frac{\partial^2 U}{\partial t^2} - \frac{c}{2} \frac{\partial^2 U}{\partial y^2} - \frac{c}{2} \frac{\partial^2 U}{\partial z^2} = 0 \quad (x = a) \quad (16b)$$

$$\frac{\partial^2 U}{\partial y \partial t} - \frac{1}{c} \frac{\partial^2 U}{\partial t^2} + \frac{c}{2} \frac{\partial^2 U}{\partial x^2} + \frac{c}{2} \frac{\partial^2 U}{\partial z^2} = 0 \quad (y = 0) \quad (16c)$$

$$\frac{\partial^2 U}{\partial y \partial t} + \frac{1}{c} \frac{\partial^2 U}{\partial t^2} - \frac{c}{2} \frac{\partial^2 U}{\partial x^2} - \frac{c}{2} \frac{\partial^2 U}{\partial z^2} = 0 \quad (y = b) \quad (16d)$$

$$\frac{\partial^2 U}{\partial z \partial t} - \frac{1}{c} \frac{\partial^2 U}{\partial t^2} + \frac{c}{2} \frac{\partial^2 U}{\partial x^2} + \frac{c}{2} \frac{\partial^2 U}{\partial y^2} = 0 \quad (z = 0) \quad (16e)$$

$$\frac{\partial^2 U}{\partial z \partial t} + \frac{1}{c} \frac{\partial^2 U}{\partial t^2} - \frac{c}{2} \frac{\partial^2 U}{\partial x^2} - \frac{c}{2} \frac{\partial^2 U}{\partial y^2} = 0 \quad (z = c) \quad (16f)$$

The numerical implementation of these conditions further involve the transformation of the differential operators to finite difference expressions. This is done according to Mur [4]. Typical transformations are (for  $x = 0$ ):

$$\frac{\partial^2 U^n(\frac{1}{2}, j, k)}{\partial x \partial t} = \frac{U^{n+1}(1, j, k) - U^{n+1}(0, j, k) - U^{n-1}(1, j, k) + U^{n-1}(0, j, k)}{2 \cdot \delta \cdot \Delta t} \quad (17a)$$

$$\frac{\partial^2 U^n(\frac{1}{2}, j, k)}{\partial t^2} = \frac{U^{n+1}(0, j, k) - 2U^n(0, j, k) + U^{n-1}(0, j, k)}{2 \cdot \Delta t^2} + \frac{U^{n+1}(1, j, k) - 2U^n(1, j, k) + U^{n-1}(1, j, k)}{2 \cdot \Delta t^2} \quad (17b)$$

$$\frac{\partial^2 U^n(\frac{1}{2}, j, k)}{\partial y^2} = \frac{U^n(0, j+1, k) - 2U^n(0, j, k) + U^n(0, j-1, k)}{2\delta^2} + \frac{U^n(1, j+1, k) - 2U^n(1, j, k) + U^n(1, j-1, k)}{2\delta^2} \quad (17c)$$

$$\frac{\partial^2 U^n(\frac{1}{2}, j, k)}{\partial z^2} = \frac{U^n(0, j, k+1) - 2U^n(0, j, k) + U^n(0, j, k-1)}{2\delta^2} + \frac{U^n(1, j, k+1) - 2U^n(1, j, k) + U^n(1, j, k-1)}{2\delta^2} \quad (17d)$$

Finally, the absorbing boundary condition at  $x = 0$  becomes

$$U^{n+1}(0, j, k) = -U^{n-1}(1, j, k) + \frac{c\Delta t - \delta}{c\Delta t + \delta} \cdot (U^{n+1}(1, j, k) + U^{n-1}(0, j, k)) \quad (18)$$

$$+ \frac{2\delta}{c\Delta t + \delta} \cdot (U^n(0, j, k) + U^n(1, j, k)) + \frac{(c\Delta t)^2}{2\delta(c\Delta t + \delta)} \cdot (U^n(0, j+1, k) + U^n(0, j-1, k) + U^n(1, j+1, k) + U^n(1, j-1, k) + U^n(0, j, k+1) + U^n(0, j, k-1) + U^n(1, j, k+1) + U^n(1, j, k-1) - 4 \cdot U^n(0, j, k) - 4 \cdot U^n(1, j, k))$$

For the other absorbing boundary conditions similar expressions can be derived.

#### 2.2.4 Sinusoidal steady state

Time stepping is continued until the desired sinusoidal steady state behaviour is achieved. The time needed to reach this state is mainly depending on the object's electrical size. The total number of time steps needed for a wave travelling at the speed of light to make two complete front-to-back-to-front traverses is normally sufficient to reach the steady state. Typical times can be found in [5]. After reaching the sinusoidal steady state the magnitude and phase of the components of the near-fields have to be determined. Due to the fact that the FD-TD method causes some fields to have a nonphysical dc offset, an algorithm is used that determines the maximum and minimum of a field component. The magnitude is calculated as  $(\max - \min)/2$  and the phase is the phase of the maximum minus an arbitrary fixed phase. To achieve a greater accuracy multiple cycles can be treated this way and an average result can be calculated.

### 2.2.5 The near-to-far field transformation

The far field data can be obtained, in principle, by solving an integral equation for the induced currents on the surface of the object. For complex objects this can be very difficult. A good alternative is to set up an equivalent problem. The object is surrounded with an arbitrary, closed, virtual boundary, the surface  $S_a$ , on which the near-field data is obtained via the FD-TD method. This surface is situated in the scattered-field region. The near-field data is used to calculate equivalent electric and magnetic surface currents on the virtual surface  $S_a$ .

$$\bar{J}_{Seq}(\bar{r}) = \hat{n} \times \bar{H}_s(\bar{r}) \quad (19a)$$

$$\bar{M}_{Seq}(\bar{r}) = -\hat{n} \times \bar{E}_s(\bar{r}) \quad (19b)$$

where  $\hat{n}$  is the outward, unit normal vector at the surface  $S_a$ , see figure 3. By making the interior of surface  $S_a$  empty with zero fields and no sources the equivalent problem is set up. The equivalent surface currents on  $S_a$  produce the same scattered field external to  $S_a$  as in the original problem.

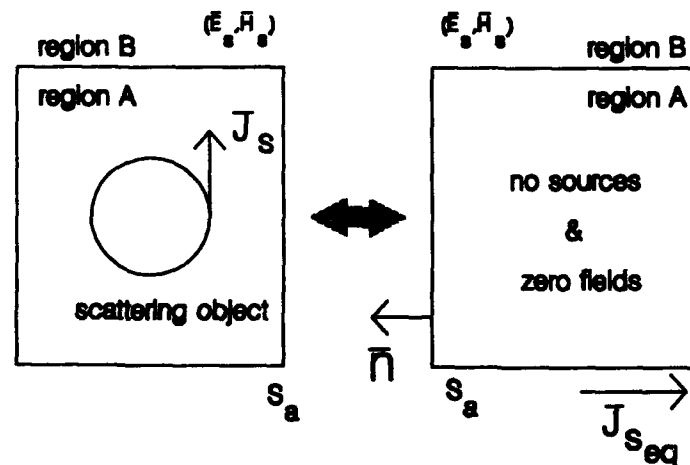


Fig. 3: The equivalent problem

The scattered far fields are given by the transform of the equivalent currents of (19a) and (19b) over the free space Green's function [6],[7]. If  $(\epsilon_0, \mu_0)$  are the region B medium characteristics with  $k_0 = 2\pi/\lambda_0$  and the free space impedance  $\eta_0 = 120\pi$  for  $\theta$  and  $\phi$  polarisations, the following scattered far fields expressions are obtained.

$$E_{\theta} = -jk_0 \eta_0 \left( A_{\theta} + \frac{F_{\theta}}{\eta_0} \right) \quad (20a)$$

$$E_{\phi} = -jk_0 \eta_0 \left( A_{\phi} - \frac{F_{\phi}}{\eta_0} \right) \quad (20b)$$

where

$$A_{\theta} = A_x \cos \theta \cos \phi + A_y \cos \theta \sin \phi - A_z \sin \theta \quad (21a)$$

$$F_{\theta} = F_x \cos \theta \cos \phi + F_y \cos \theta \sin \phi - F_z \sin \theta \quad (21b)$$

$$A_{\phi} = -A_x \sin \phi + A_y \cos \phi \quad (21c)$$

$$F_{\phi} = -F_x \sin \phi + F_y \cos \phi \quad (21d)$$

and the potentials in the far field region are given by

$$\begin{bmatrix} \bar{A} \\ \bar{F} \end{bmatrix} = \frac{e^{-jk_0 r}}{4\pi r} \iint_{S_a} \begin{bmatrix} \bar{J}_{Seq} \\ \bar{M}_{Seq} \end{bmatrix} e^{jk_0 r \cos \xi} dS_a \quad (22a)$$

with

$$r \cos \xi = (x \cos \phi + y \sin \phi) \sin \theta + z \cos \theta \quad (22b)$$

The radar cross section RCS is calculated as the ratio

$$RCS = 4\pi r^2 \left( \frac{E_{\theta}^2 + E_{\phi}^2}{E_{\theta}^{i2} + E_{\phi}^{i2}} \right) \quad r \rightarrow \infty \quad (23)$$

where  $E_{\theta}^i$  and  $E_{\phi}^i$  are the corresponding components of the incident plane wave. The complete bistatic RCS is a natural result of this procedure for a given incident angle and polarisation of the illuminating wave.

### 3 FD-TD COMPUTED SCATTERING AND PENETRATION PROBLEMS

The used 3-dimensional FD-TD code is a Fortran code. It is used on a Convex C230 supercomputer with vectorisation and parallelisation turned on. Typical computation times for one RCS value are

$$T = 1.3 \cdot N \cdot (1.7 \cdot 10^{-6} D^3 + 2.7 \cdot 10^{-5} D^2 + 2.9 \cdot 10^{-3} D) \quad (24)$$

where T is the computation time in seconds, N is the total number of time steps and D is the cube root of the total number of grid cells. The memory requirements are empirically determined at

$$M = 7.3 \cdot 10^{-5} D^3 + 1.2 \cdot 10^{-3} D^2 + 0.8 \quad (25)$$

where M is the number of megabytes needed by the FD-TD code for single precision calculations.

### 3.1 Radar cross section of a square metal plate

In this section results are shown for the FD-TD computed monostatic radar cross section of a perfectly conducting square plate. The results are compared with the results of a code that uses physical optics and diffraction theory.

The plate spans  $6\lambda \times 6\lambda$  and as  $\delta$  is chosen  $\lambda/10$  the plate is formed by  $60 \times 60 \times 1$  cells. The absorbing boundary is located at a uniform distance of 10 cells from the plate surface. The geometry of the plate is shown in figure 4. Vertical polarisation of the incident wave is used. Azimuth angles are from  $0^\circ$  to  $10^\circ$  with the elevation angle fixed at  $90^\circ$ .

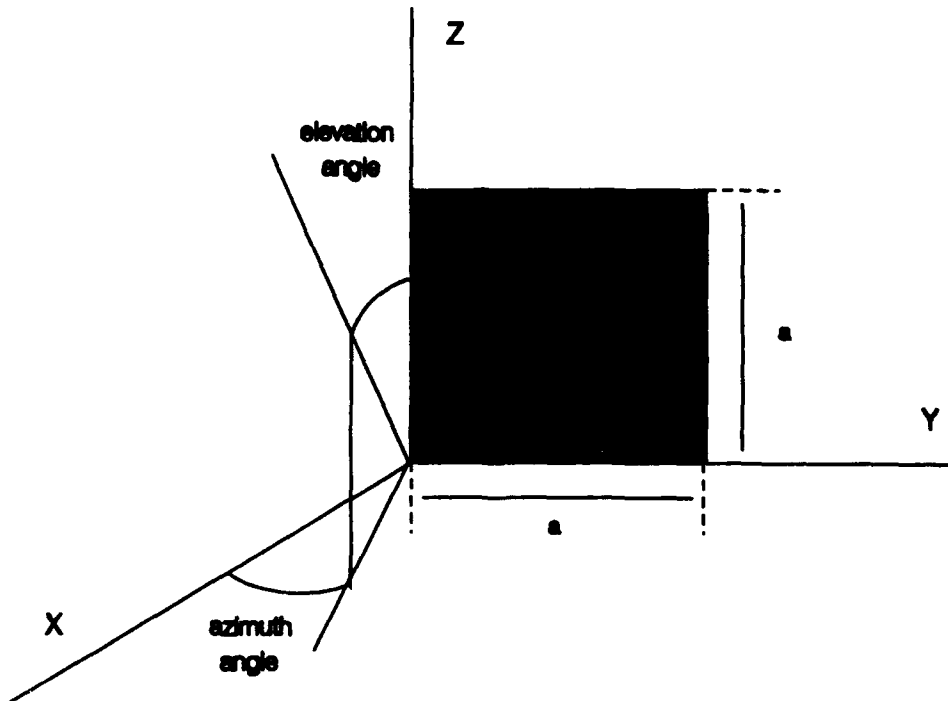


Fig. 4: Geometry of the plate

The results are presented in figure 5, which shows excellent agreement between the two methods at the maxima within 1 dBsm. At the negative going peaks a greater deviation is noticed, due to the imperfections embedded in the two methods. However, for practical applications only the maxima and the positions of the minima are important, not the absolute values of the minima.

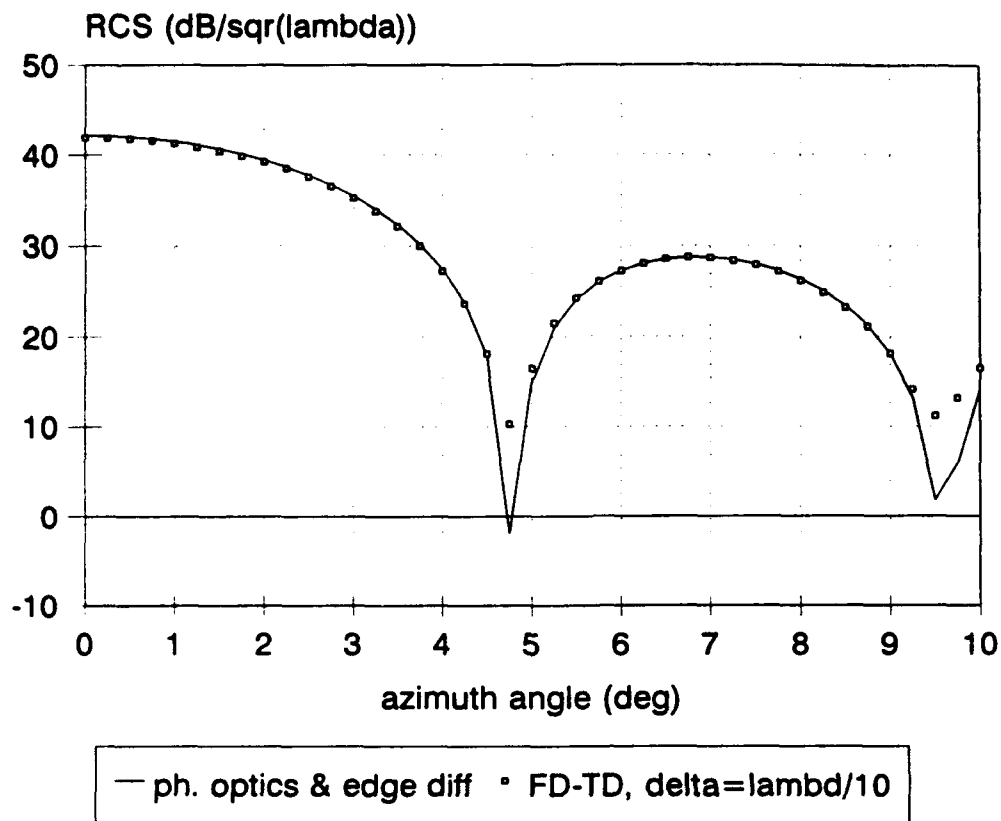


Fig. 5: Results for a square metal plate,  $6\lambda \times 6\lambda$ , vertical polarisation

### 3.2 Radar cross section of a rectangular metal cavity.

#### 3.2.1 Vertical polarisation of the incident wave

We next consider the target shown in figure 6. The shown cavity is formed by a perfectly conducting cube with one side removed.

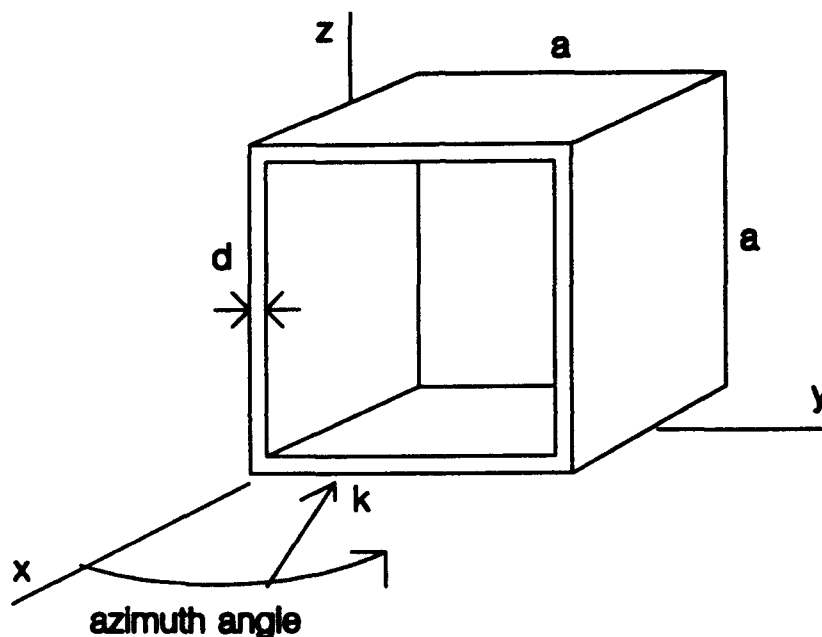


Fig. 6: Geometry of the metal cavity

The cavity is illuminated by a vertical polarised plane wave with a frequency of 15 GHz. The dimensions of the cavity as shown in figure 6 are  $a = 19.9$  mm and  $d = 0.96$  mm. Using  $\delta = 0.4975$  mm  $\approx \lambda/40$  and forming the cavity by  $a = 40$  cells and  $d = 2$  cells is a good discretisation of the cavity. The FD-TD computed monostatic radar cross section versus azimuth angle is compared to measurements made in the anechoic chamber facility at FEL-TNO. Measurements are made according to [8]. The calibrated background level in the anechoic room was below -55 dBsm. The elevation angle is fixed at  $90^\circ$ .

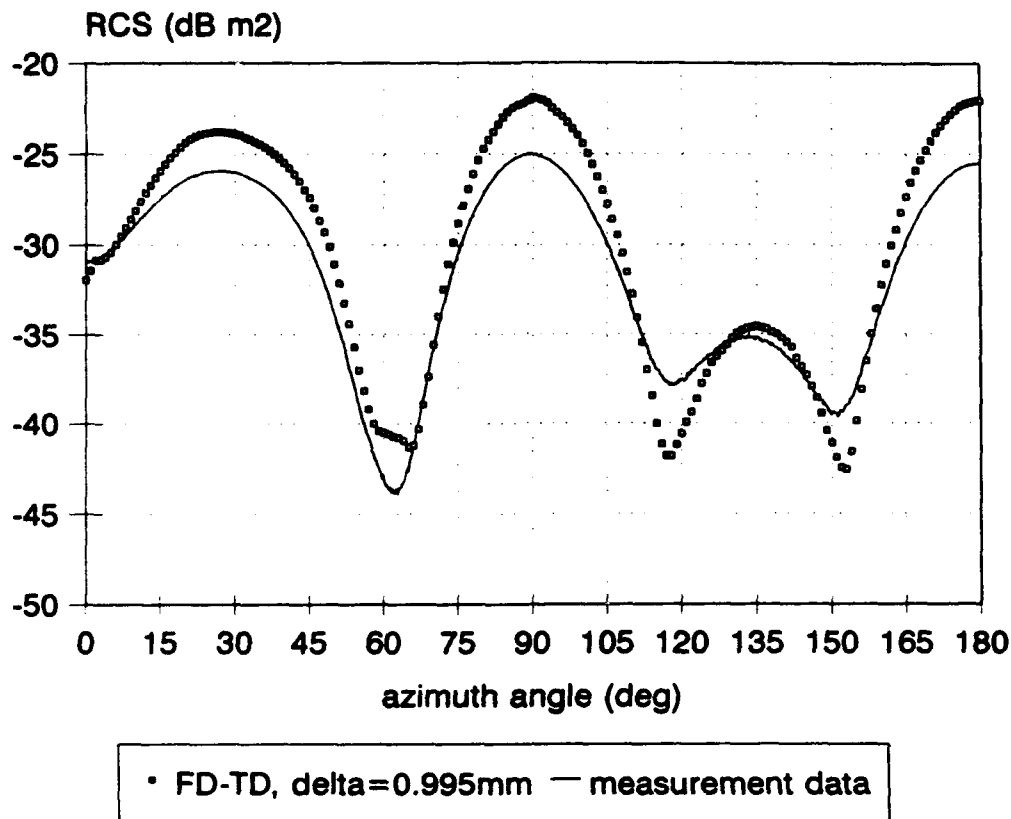


Fig. 7: Measurement versus FD-TD code for a metal cavity, vertical polarisation of incident wave

Figure 7 shows a reasonable agreement between FD-TD data and measurement data, within 3 dB. However, care must be taken because the measurement data is not as expected. At an angle of 180°, the rear of the cavity, the object behaves as a flat conducting plate which has a well defined monostatic radar cross section of approximately -23 dBsm which shows more agreement with the FD-TD data than with the measurement data. Apparently, the only deviation is an offset of about -2 dBsm on the measurement data relative to the FD-TD results. For the remainder the patterns seem to be matching. This offset is probably caused by a calibration error for the reference target used during the measurements. For the calibration a sphere was used which had an RCS value of only 4 to 8 dB above the background level. This can result in a wrong RCS value for the reference object which explains the observed offset.

FD-TD calculations using  $\delta = 0.995 \text{ mm} = \lambda/20$  and forming the cavity by  $a = 20$  cells and  $d = 1$  cell, show, when compared to the former FD-TD result, that this change in resolution gives only a slight change in RCS pattern. Figure 8 shows that choosing  $\delta = \lambda/20$  seems to be sufficient to model the cavity with good accuracy.

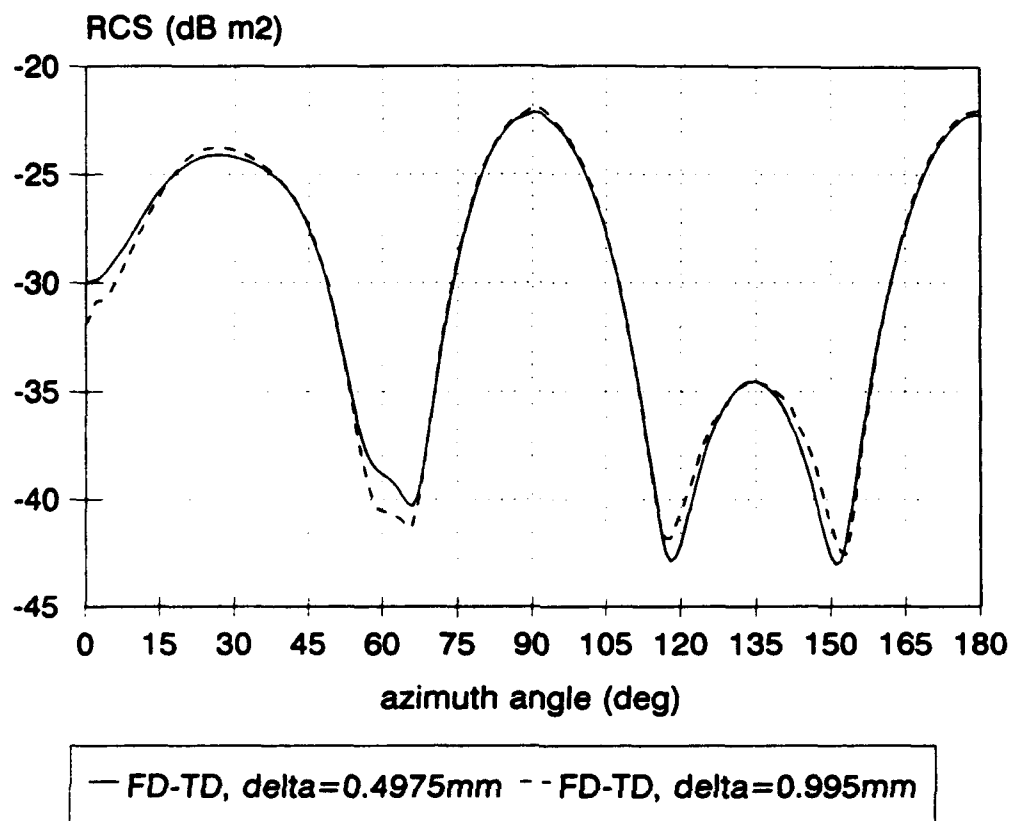


Fig. 8: The influence of the grid resolution on the FD-TD results for a metal cavity, vertical polarised incident wave

### 3.2.2 Horizontal polarisation of the incident wave

We now consider the same cavity as used before illuminated by a horizontal polarised plane wave. Using again  $\delta = \lambda/40$  figure 9 shows that the FD-TD computed radar cross section pattern shows good agreement with the measurement data except for an offset on the measurement data of approximately -7 dBsm.

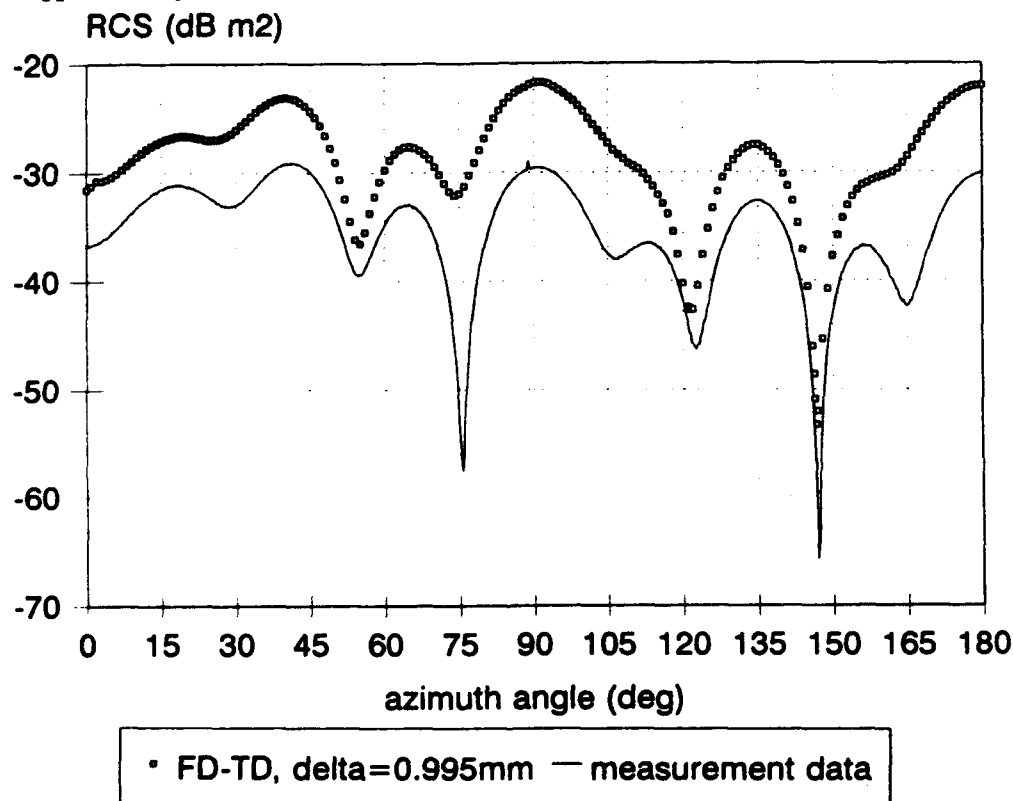


Fig. 9: Measurement versus FD-TD code for a metal cavity, horizontal polarisation of the incident wave

Again it is assumed that the measurement data are incorrect due to the calibration error mentioned in the previous section. A clue that states this conclusion is the fact that the radar cross section at an azimuth angle of  $180^\circ$ , which is perpendicular incidence, should be independent of the polarisation of the incident wave because at this angle the cavity is symmetric for rotations of  $90^\circ$  along the x-axis. The FD-TD calculations are in agreement with this fact but the measurements show a discrepancy of almost 5 dBsm between horizontal and vertical polarisations. Assuming the FD-TD calculations are correct, a comparison is made with FD-TD calculations using a grid

resolution of  $\delta = \lambda/20$ . Figure 10 shows that the results again are only slightly different between both discretisations.

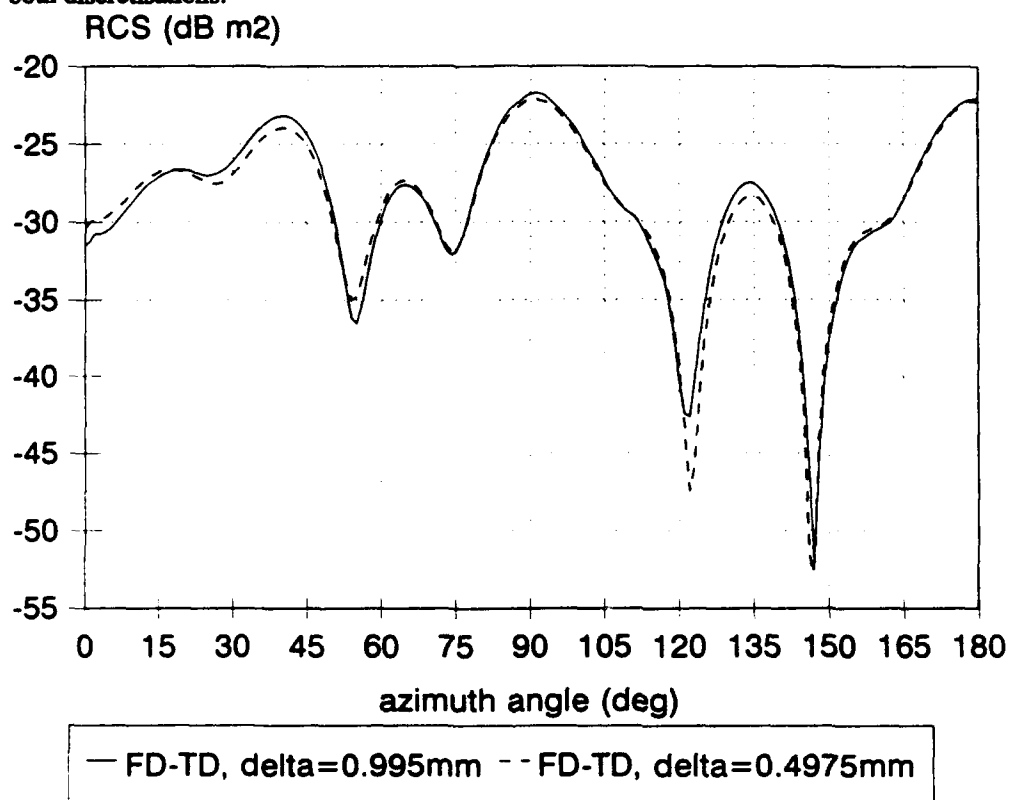


Fig. 10: The influence of the grid resolution on the FD-TD results for a metal cavity, horizontal polarised incident wave

### 3.3 Radar cross section of a metal wedge

#### 3.3.1 Vertical polarisation of incident wave

The next analyzed target is a perfectly conducting wedge with an opening angle of  $10^\circ$  as shown in figure 11. At a frequency of 15 GHz side  $a$  is dimensioned to be  $5\lambda$ . Choosing  $\delta$  to be  $\lambda/20$  the length  $a$  is formed by 100 cells. Again the boundary is only 10 cells away from the outer dimensions of the wedge.

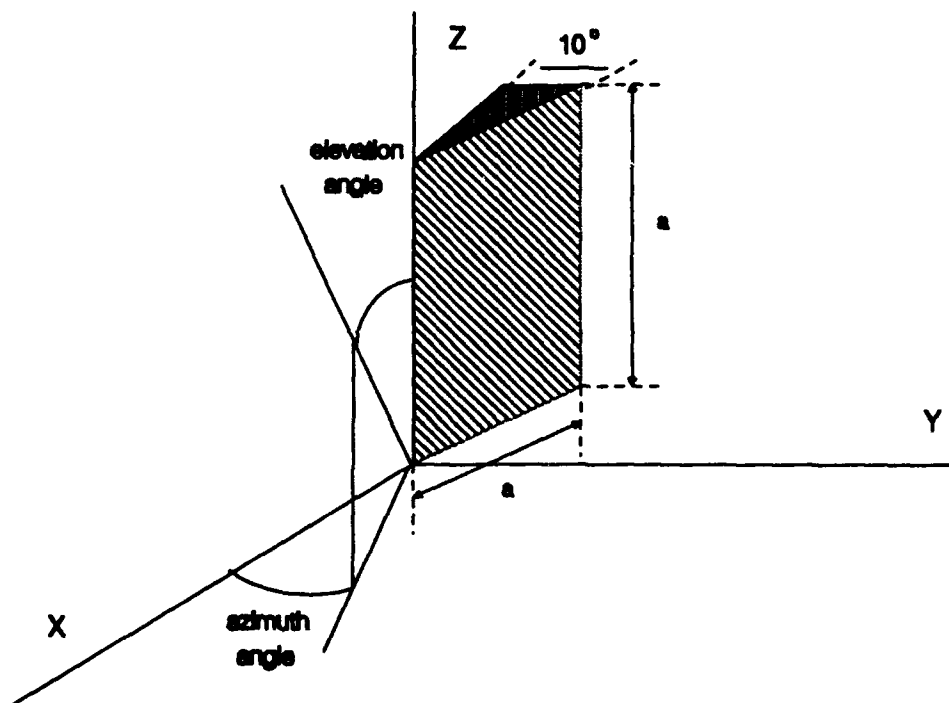


Fig. 11: Geometry of the wedge

The central axis of the wedge is positioned parallel to the x-axis. The computed FD-TD result for a vertical polarised incident wave is shown in figure 12 together with the experimental results obtained at the anechoic chamber facility at FEL-TNO. The elevation angle is fixed at  $90^\circ$ .

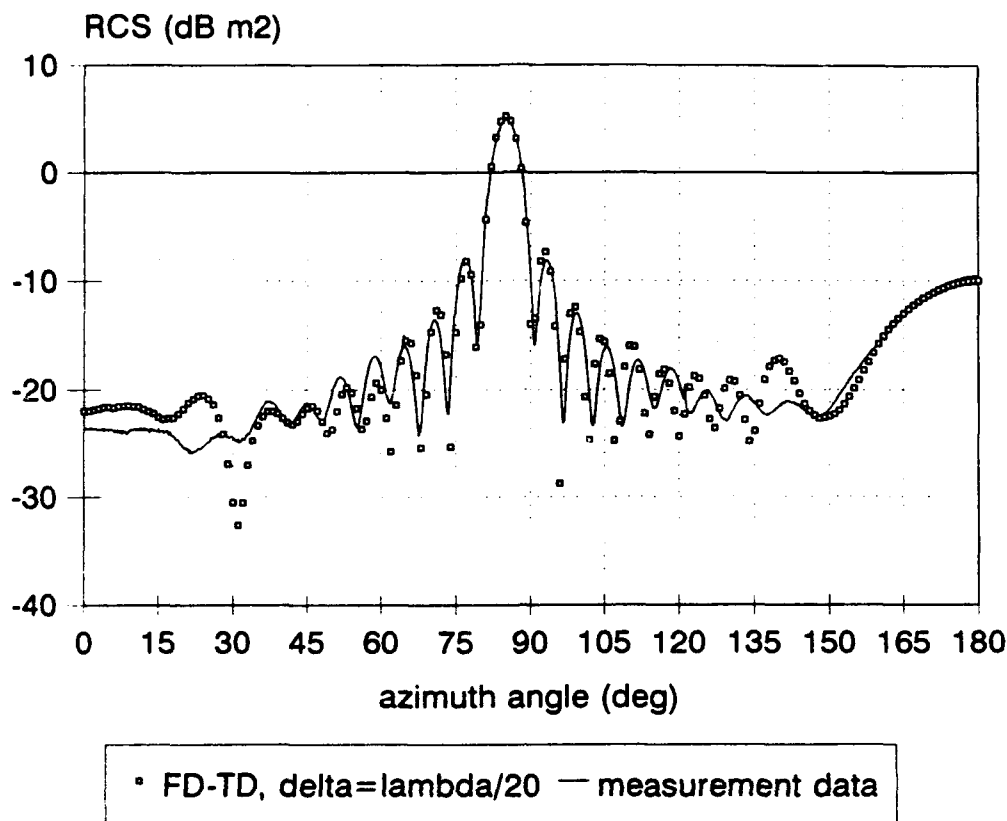


Fig. 12: Measurement versus FD-TD code for a metal wedge, vertical polarised incident wave

A good agreement is obtained for the main lobe at  $85^\circ$  and the first second and third side lobe. At the angles around  $30^\circ$  and  $140^\circ$  the FD-TD method gives wrong radar cross section values. These are probably due to the fact that the two planes forming the wedge, are making an angle with the grid of only  $5^\circ$ . Such a small angle has a very poor discrete representation. To show this effect the wedge is positioned as in figure 13. The same experiment is repeated and the results are shown in figure 14. An improvement can be noticed at azimuth angles around  $30^\circ$  and  $140^\circ$ . This improvement will become even more obvious in the next paragraph as the wedge is illuminated by a horizontal polarised plane wave.

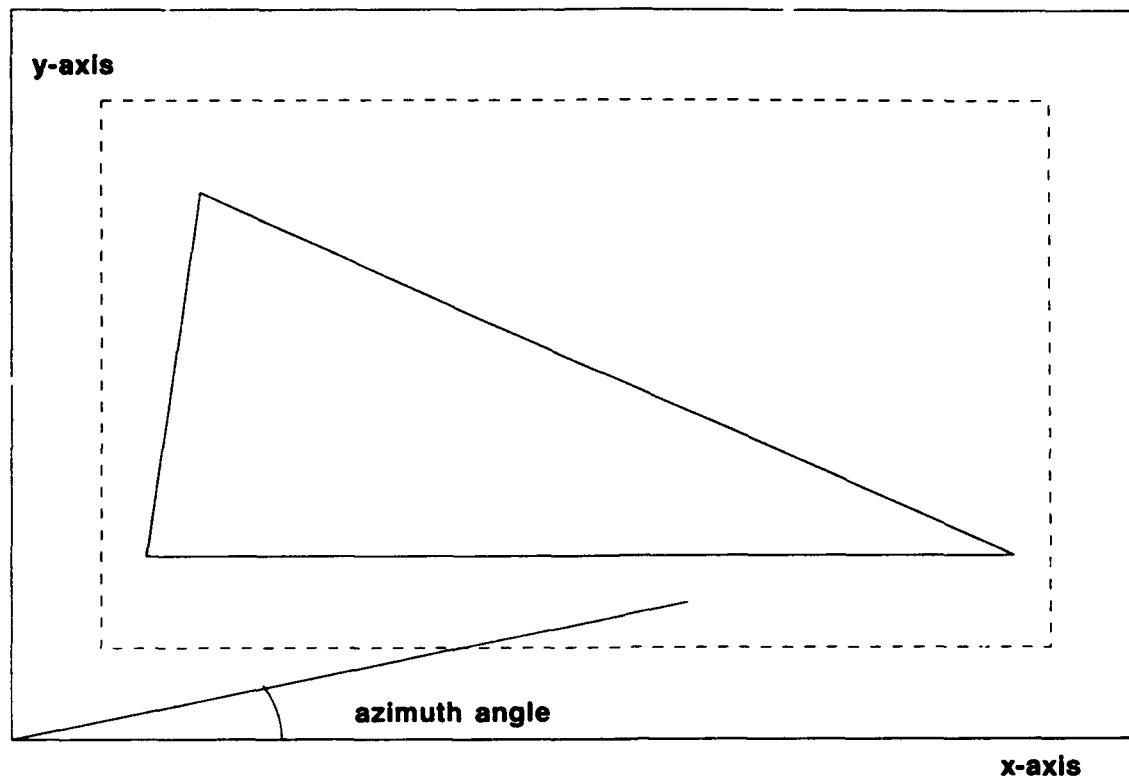


Fig. 13: Improved position of the wedge in the grid  
RCS (dB m<sup>2</sup>)

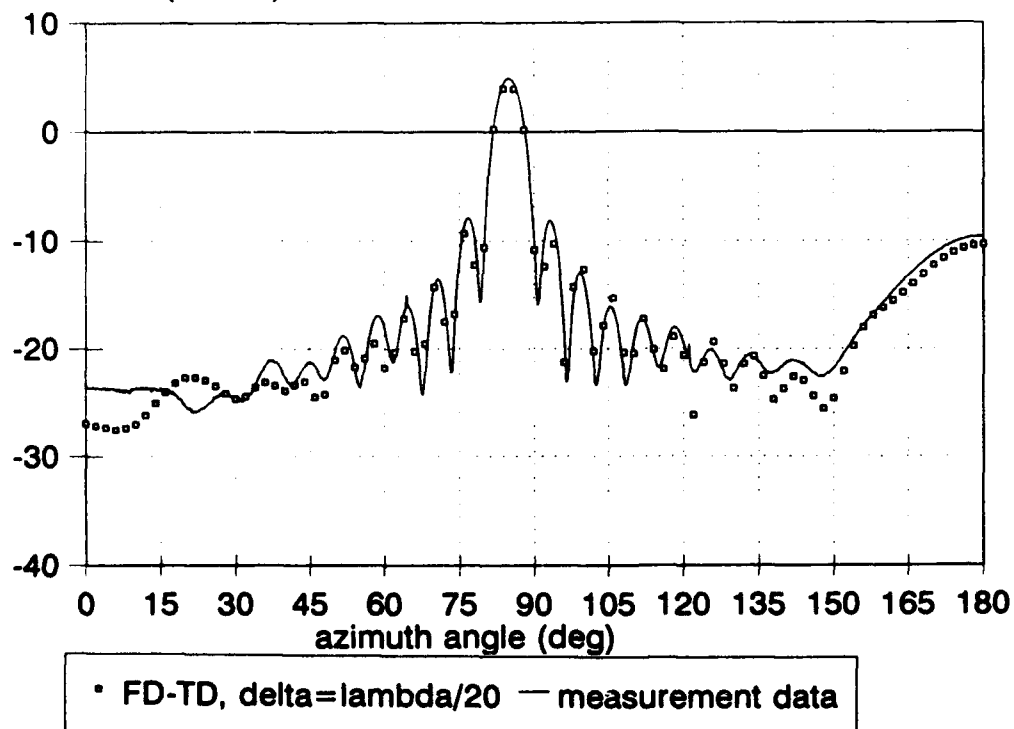


Fig. 14: Measurement versus FD-TD code for a metal wedge with an improved positioning in the grid, vertical polarised incident wave

### 3.3.2 Horizontal polarisation of the incident wave

As in the previous chapter the wedge is analyzed with the 3D FD-TD code in two ways; One with the central axis of the wedge parallel to the x-axis and the second one with one plane of the wedge parallel to the x-axis as in figure 13. This time a horizontal polarisation of the incident wave is used. The results are shown respectively in figure 15 and figure 16. Again good results are obtained for certain angles. When analyzing these two figures it becomes very obvious that the positioning of the wedge in the grid has a major effect on the computed RCS value at those angles where interference of the reflection of two planes of the wedge becomes dominant.

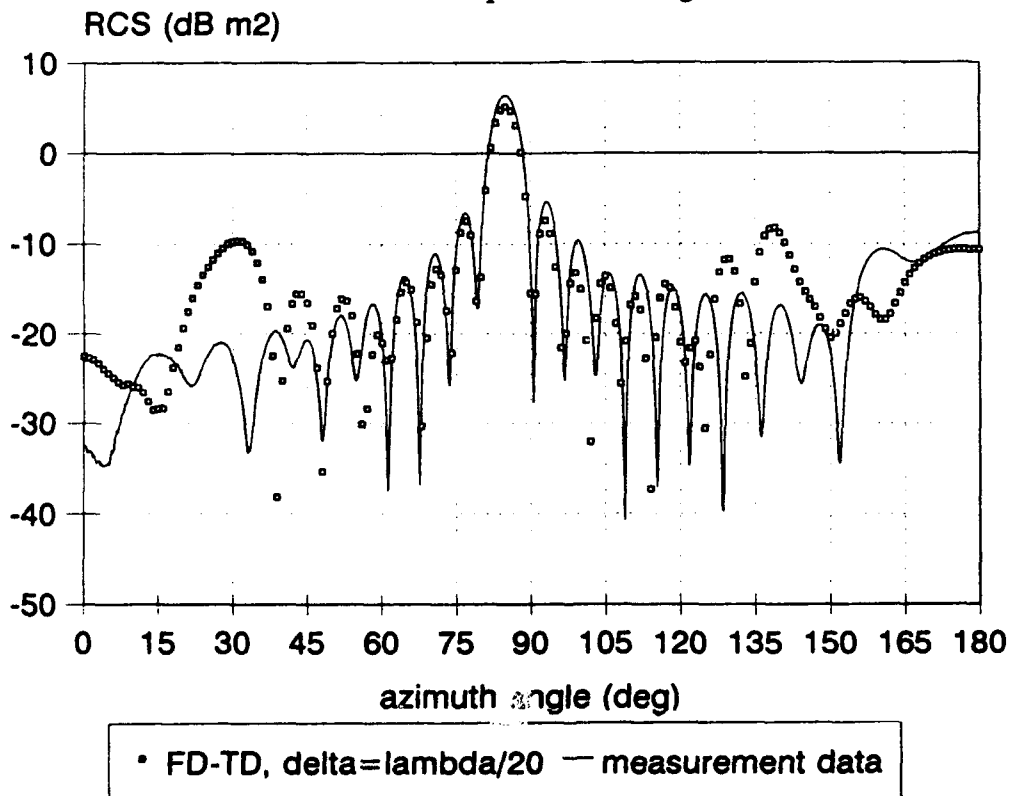
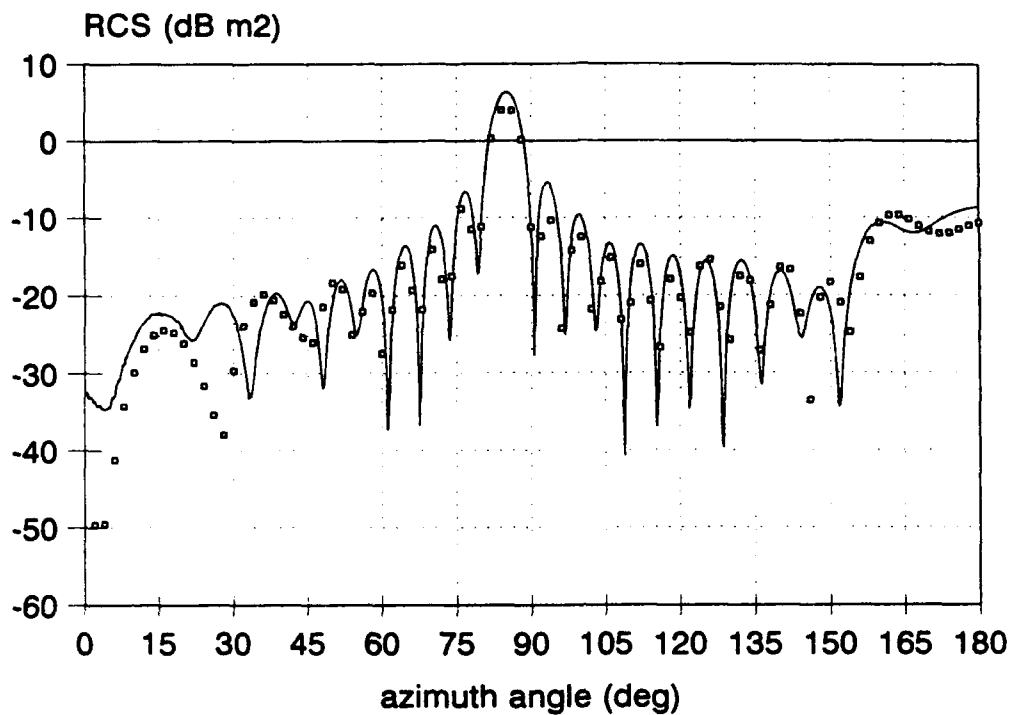


Fig. 15: Measurement versus FD-TD code for a metal wedge, horizontal polarised incident wave



• FD-TD,  $\Delta = \lambda/20$  — measurement data

Fig. 16: Measurement versus FD-TD code for a metal wedge with an improved position in the grid, horizontal polarised incident wave

### 3.4 Field penetration in a lossy inhomogeneous sphere

The last object to be analyzed is a lossy inhomogeneous dielectric sphere which consists of a core and a shell. The core, marked in figure 17 with 1, has the following characteristics:  $\epsilon_{r1} = 72$ ,  $\sigma_1 = 0.9$  S/m and  $a_1 = 0.08$  m. For the shell, marked with 2, these values are:  $\epsilon_{r2} = 7.5$ ,  $\sigma_2 = 0.05$  S/m and  $a_2 = 0.15$  m.

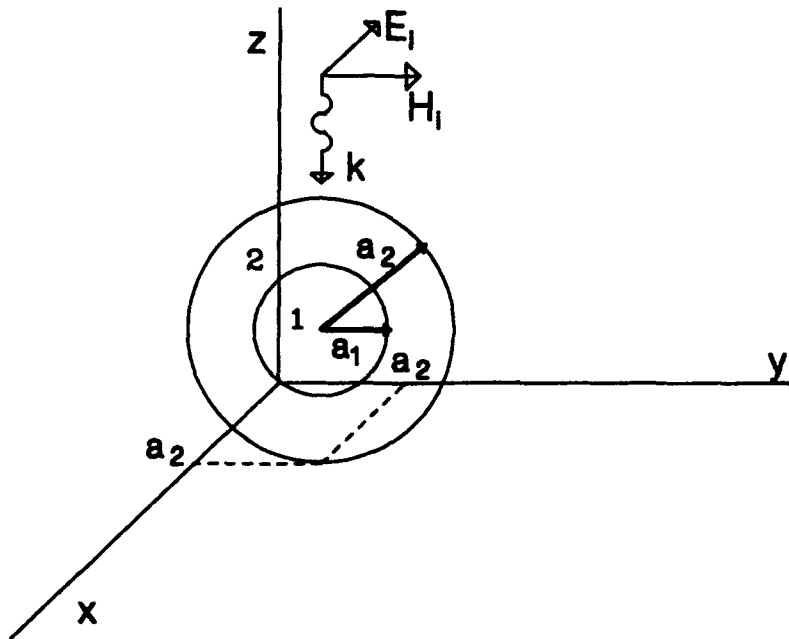
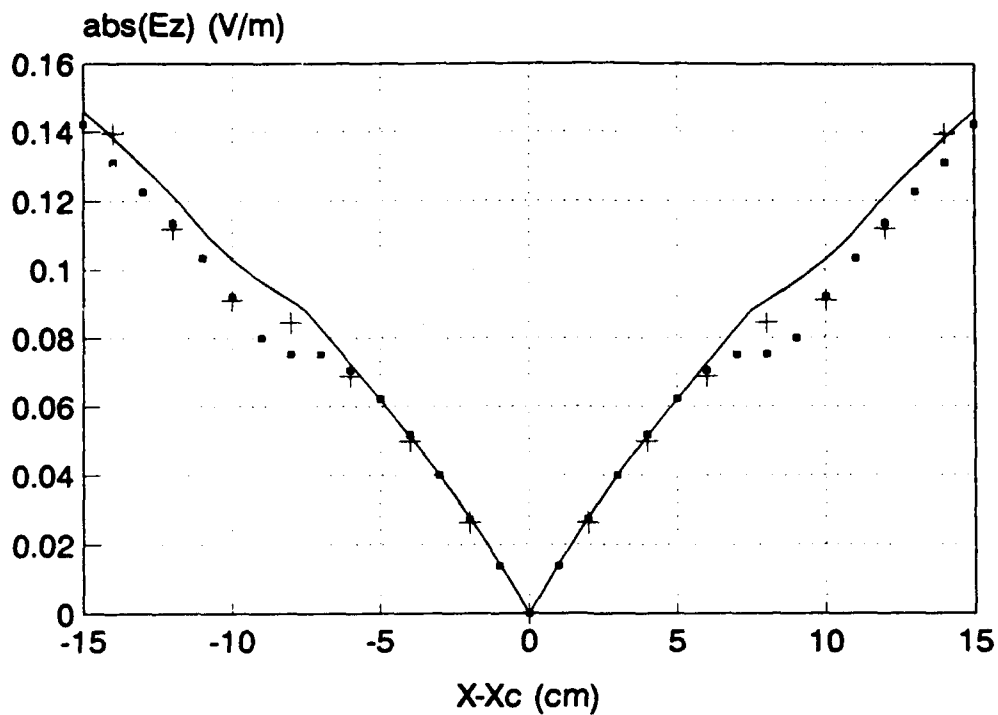


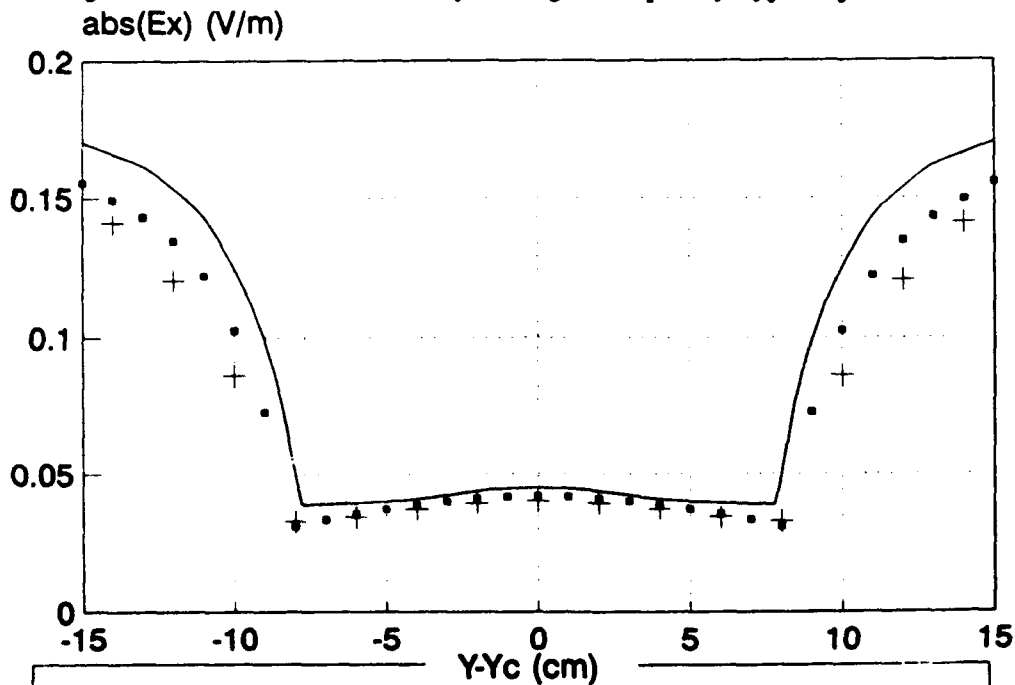
Fig. 17: Geometry of the lossy inhomogeneous sphere

The incident plane wave is travelling in the negative z-direction and has an E component in the negative x-direction and an H component in the y-direction as in figure 17. The centre of the sphere  $(x_c, y_c, z_c)$  lies at  $(a_2, a_2, a_2)$ . This electromagnetic problem has an analytical solution that can be obtained with the Mie series [9]. The magnitudes of the field components of the electrical field in the sphere are computed with the FD-TD code and compared with the analytical solution. A frequency of 100 MHz is used and the sphere is discretised at two resolutions,  $\delta = 0.01$  m and  $\delta = 0.02$  m.



• FD-TD, delta=1cm + FD-TD, delta=2cm — exact solution

Fig. 18: Ez versus x inside a lossy inhomogeneous sphere,  $y = y_c$ ,  $z = z_c$



• FD-TD, delta=1cm + FD-TD, delta=2cm — exact solution

Fig. 19: Ex versus y inside a lossy inhomogeneous sphere,  $x = x_c$ ,  $z = z_c$

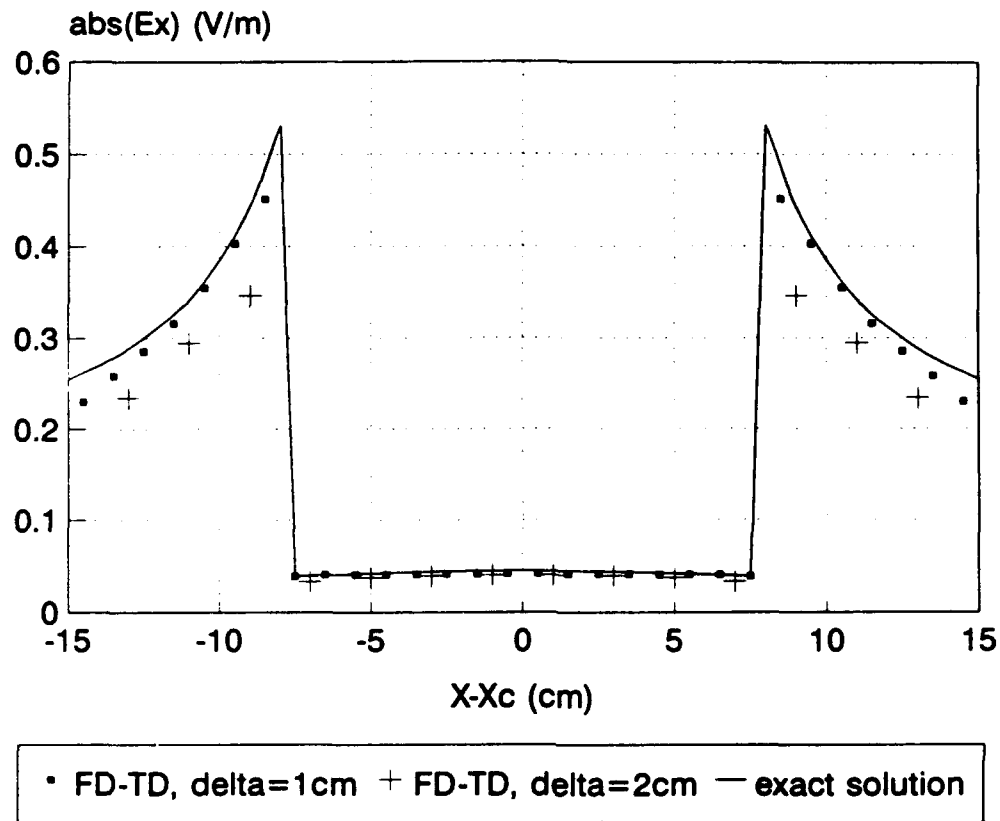


Fig. 20: Ex versus x inside a lossy inhomogeneous sphere,  $y = y_c$ ,  $z = z_c$

These figures show a good agreement between the FD-TD computed results and the analytical solution. It becomes clear that at sufficiently high resolutions FD-TD is able to model field penetration in lossy dielectric objects with high contrasts.

## 4

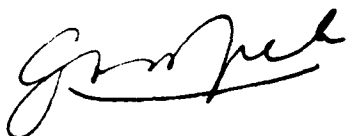
## CONCLUSIONS

The 3-dimensional FD-TD method is a useful method for analyzing problems of scattering and penetration of electromagnetic waves. With modern supercomputers, scattering from objects with maximum dimensions of less than 10 wavelengths can be analyzed with this method. Depending on the complexity of the shape and the materials used these dimensions may become smaller. Good results are obtained for  $\delta = \lambda/10$  to  $\delta = \lambda/40$  depending on the complexity of the object of interest. For perfectly conducting objects that fit exactly in the lattice,  $\delta = \lambda/20$  seems to be sufficient to model the RCS with 1 dB accuracy. For other objects a higher discretisation has to be used.

## LITERATURE

- [1] K.S. Yee,  
"Numerical solution of initial boundary value problems involving Maxwell's equations in isotropic media",  
IEEE Trans. antennas and propagation, Vol. AP-14, No. 3, May 1966, pp.302-307.
- [2] A. Taflove and M.E. Brodwin,  
"Numerical solution of steady state electromagnetic scattering problems using the time dependent Maxwell's equations",  
IEEE Trans. microwave theory tech., Vol. MTT-23, Aug. 1975, pp.623-630.
- [3] B. Engquist and A. Majda,  
"Absorbing boundary conditions for the numerical solution of waves",  
Math. comp. 31, 1977, pp.629-651.
- [4] G. Mur,  
"Absorbing boundary conditions for the finite difference approximation of the time domain electromagnetic field equations",  
IEEE Trans. electromagn. compat., EMC-23, 1981, pp.377-382.
- [5] A. Taflove and K.R. Umashankar,  
"Review of FD-TD numerical modeling of electromagnetic wave scattering and radar cross section",  
Proceedings of the IEEE, Vol. 77, No. 5, May 1989, pp.682-699.
- [6] J. van Bladel,  
"Electromagnetic fields",  
McGraw Hill, New York, 1964.
- [7] R.F. Harrington,  
"Time harmonic electromagnetic fields",  
McGraw Hill, New York, 1961, ch. 3.
- [8] "Radar cross section measurements with the HP 8510B network analyzer",  
HP application note 8510-2.
- [9] J.A. Kong,  
"Electromagnetic wave theory",  
John Wiley and Sons, New York, 1986.

---



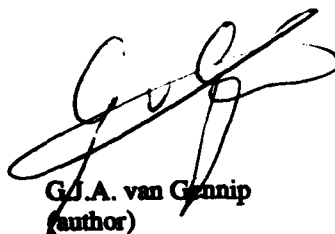
G.A. van der Spek  
(group leader)

---



H.J.M. Heemskerk  
(project leader)

---



G.J.A. van Gennip  
(author)

## REPORT DOCUMENTATION PAGE

(MOD-NL)

- 
- |  |                                 |   |
|--|---------------------------------|---|
| 1. DEFENSE REPORT NUMBER (MOD-NL)<br>TD92-1762 | 2. RECIPIENT'S ACCESSION NUMBER | 3. PERFORMING ORGANIZATION REPORT NUMBER<br>FEL-92-B190 |
|--|---------------------------------|---|
- 
- |  |                         |                             |
|--|-------------------------|-----------------------------|
| 4. PROJECT/TASK/WORK UNIT NO.<br>20369 | 5. CONTRACT NUMBER<br>- | 6. REPORT DATE<br>JUNE 1992 |
|--|-------------------------|-----------------------------|
- 
- |  |                              |   |
|--|------------------------------|---|
| 7. NUMBER OF PAGES<br>35 (EXCL. RDP,<br>EXCL. DISTRIBUTION LIST) | 8. NUMBER OF REFERENCES<br>9 | 9. TYPE OF REPORT AND DATES COVERED<br>FINAL REPORT |
|--|------------------------------|---|
- 
10. TITLE AND SUBTITLE  
THEORY AND APPLICATIONS OF THE 3-DIMENSIONAL FINITE-DIFFERENCE TIME-DOMAIN METHOD
- 
11. AUTHOR(S)  
G.J.A. VAN GENNIP
- 
12. PERFORMING ORGANIZATION NAME(S) AND ADDRESS(ES)  
TNO PHYSICS AND ELECTRONICS LABORATORY, P.O. BOX 96864, 2509 JG THE HAGUE  
OUDERWAALSDORPERWEG 63, THE HAGUE, THE NETHERLANDS
- 
13. SPONSORING/MONITORING AGENCY NAME(S)
- 
14. SUPPLEMENTARY NOTES
- 
15. ABSTRACT (MAXIMUM 200 WORDS, 1044 POSITIONS)  
THE 3-DIMENSIONAL FINITE-DIFFERENCE TIME-DOMAIN METHOD IS A NUMERICAL METHOD FOR SOLVING ELECTROMAGNETIC PENETRATION AND SCATTERING PROBLEMS. IT USES A FINITE DIFFERENCE REPRESENTATION OF THE TIME DEPENDENT MAXWELL EQUATIONS. THE OBJECT OF INTEREST IS EMBEDDED IN A LATTICE AND THE TIME IS DIVIDED IN DISCRETE INTERVALS. BY APPLYING THE FINITE-DIFFERENCE EQUATIONS FOR EVERY TIME STEP THE PROPAGATION AND SCATTERING OF WAVES IS SIMULATED. IN THIS REPORT THE 3-DIMENSIONAL FD-TD METHOD AND ITS ALGORITHMS ARE EXPLAINED. RESULTS ARE PRESENTED FOR A PERFECTLY CONDUCTING PLATE, CUBE AND WEDGE AND FOR A DIELECTRIC LAYERED SPHERE. THE CALCULATED RESULTS AGREE WITH EXPERIMENTAL AND EXACT THEORETICAL RESULTS.
- 
- |   |  |
|---|--|
| 16. DESCRIPTORS<br>NUMERICAL COMPUTATIONS<br>SCATTERING OF ELECTROMAGNETIC WAVES<br>RADAR CROSS SECTION | IDENTIFIERS<br>FINITE DIFFERENCE METHOD<br>MAXWELL EQUATION<br>TIME DOMAIN METHOD<br>BOUNDARY CONDITIONS |
|---|--|
- 
- |   |   |   |
|---|---|---|
| 17a. SECURITY CLASSIFICATION<br>(OF REPORT)<br>UNCLASSIFIED | 17b. SECURITY CLASSIFICATION<br>(OF PAGE)<br>UNCLASSIFIED | 17c. SECURITY CLASSIFICATION<br>(OF ABSTRACT)<br>UNCLASSIFIED |
|---|---|---|
- 
- |   |   |
|---|---|
| 18. DISTRIBUTION/AVAILABILITY STATEMENT<br>UNLIMITED AVAILABILITY | 17d. SECURITY CLASSIFICATION<br>(OF TITLES)<br>UNCLASSIFIED |
|---|---|
-